Investigation on the thermal expansion behavior of FeCoNi and Fe30Co30Ni30Cr10-xMnx high entropy alloys

Chun-Lin Lin, Jhuo-Lun Lee, Shih-Ming Kuo, Ming-Yen Li, Lu Gan, Hideyuki Murakami, Seiji Mitani, Stéphane Gorsse, An-Chou Yeh

Materials Chemistry and Physics XXX (XXXX) XXXXXX

Contents lists available at ScienceDirect

Materials Chemistry and Physics

journal homepage: www.elsevier.com/locate/matchemphys

Investigation on the thermal expansion behavior of FeCoNi and $Fe_{30}Co_{30}Ni_{30}Cr_{10-x}Mn_x$ high entropy alloys

Chun-Lin Lin [a,b], Jhuo-Lun Lee [a,c], Shih-Ming Kuo [d], Ming-Yen Li [d], Lu Gan [b], Hideyuki Murakami [b,e], Seiji Mitani [b], Stéphane Gorsse [f], An-Chou Yeh [a,c,*]

[a] Department of Materials Science and Engineering, National Tsing Hua University, 101, Sec. 2, Kuang-Fu Road, Hsinchu, 30013, Taiwan
[b] National Institute for Materials Science, Sengen 1-2-1, Tsukuba, Ibaraki, 305-0047, Japan
[c] High Entropy Materials Center, National Tsing Hua University, 101, Sec. 2, Kuang-Fu 10 Road, Hsinchu, 30013, Taiwan
[d] New Materials Research & Development Department, China Steel Corporation, 1, Chung Kang Rd., Hsiao Kang, Kaohsiung, 81233, Taiwan
[e] Department of Nanoscience and Nanoengineering, Graduate School of Advanced Science and Engineering, Waseda University, 3-4-1, Okubo, Shinjuku-ku, 169-8555, Japan
[f] CNRS, Univ. Bordeaux, Bordeaux INP, ICMCB, UMR 5026, F-33600, Pessac, France

HIGHLIGHTS

- The suppressed expansion behaviors in some high entropy alloy are presented.
- Replacing Mn with Cr can lead to decrease in thermal expansion.
- Replacing Mn with Cr can lead to decrease in saturation magnetization.
- Replacing Mn with Cr can lead to decrease in Curie temperature.
- Higher configurational entropy results larger sum of magnetic entropy difference.

ARTICLE INFO

Keywords:
Coefficient of thermal expansion
High entropy alloy
Curie temperature
Invar effect

ABSTRACT

This work investigates the thermal expansion behaviors of $Fe_{30}Co_{30}Ni_{30}Cr_{10-x}Mn_x$ High Entropy Alloys (HEAs) (x = 0, 5, 10 at.%) from 400 K to 1200 K. Interestingly, comparing to that of Cantor alloy, a decrease in Cr and Mn in Co–Cr–Fe–Mn–Ni system could significantly decrease the thermal expansion coefficient by 45.2%; $Fe_{30}Co_{30}Ni_{30}Cr_{10-x}Mn_x$ (x = 0, 5, 10) also showed an abrupt change in thermal expansion behaviors similar to that of Invar alloys. Experimental and theoretical analysis suggest the abrupt change in thermal expansion behaviors of these HEAs were associated with the transition from ferromagnetism to paramagnetism, and these alloys appear to exhibit the dimensional stability of the Invar effect. Since the Invar effect is related to ferromagnetic properties, the amount of Cr and Mn in the HEAs would influence the suppression of thermal expansion due to different intensity of anti-ferromagnetic coupling effect. This research contributes to the understanding of the thermal expansion behaviors of Co–Cr–Fe–Mn–Ni high entropy alloys and the effects of antiferromagnetic elements.

1. Introduction

Thermal expansion behaviors of metal alloys can be influenced by non-equilibrium vacancy concentration, atomic bonding, and Invar effects [1–5]. Among them, Invar effect was firstly reported in Invar 36 alloy by Guillaume in 1897 [6]. Although the mechanism of the Invar effect remains controversial, the effect is known to relate to the ferromagnetic property and the crystal structure of the alloy [2,7,8]. Low Coefficient of Thermal Expansion (CTE) alloys such as HRA929 (developed by Hitachi Metals, Ltd.) [9], Incoloy 903, Incoloy 909 (developed

* Corresponding author. Department of Materials Science and Engineering, National Tsing Hua University, 101, Sec. 2, Kuang-Fu Road, Hsinchu, 30013, Taiwan.
E-mail addresses: oscar100031230@gmail.com (C.-L. Lin), a0920989910@gmail.com (J.-L. Lee), 172767@mail.csc.com.tw (S.-M. Kuo), 167916@mail.csc.com.tw (M.-Y. Li), gan.lu@nims.go.jp (L. Gan), murakami.hideyuki@nims.go.jp (H. Murakami), MITANI.Seiji@nims.go.jp (S. Mitani), sgorsse@gmail.com (S. Gorsse), yehac@mx.nthu.edu.tw (A.-C. Yeh).

Special Metals Corporation) [10], and Thermo-Span alloy (developed by Carpenter Technology Corporation) [11] are important for engineering applications that require dimensional stability at temperatures around 673 K, however, Cr content of these alloys are kept low due to its anti-ferromagnetic coupling effect which would adversely affect the low CTE behavior [2,7,9]; since Cr content is important for high temperature oxidation resistance, the temperatures of application of these alloys are limited by the low or zero Cr content [12,13]. Recently, the development of High Entropy Alloys (HEAs) presents a wide composition scope for achieving desired physical properties, such as a combination of strength and ductility, phase stability, and tunable ferromagnetic behavior [14–21]. To the best of the authors' knowledge, there are limited literatures reporting the CTE behaviors of HEAs, examples are $Al_xCoCrFeNi$ (7.97–13.39 ppm/K, at 450 K) [22], AlCoCrFe (4–12 ppm/K, from 300 to 400 K) [23], medium-entropy subsystems of the CrMnFeCoNi HEAs (7–23 ppm/K, from 100 to 700 K) [24] and FeCoNi medium entropy alloys (7–12 ppm/K, from 273 to 993 K) [25], these HEAs can exhibit suppressed CTE at elevated temperatures, however, the underlying mechanism remains unclear to-date. The well-known equiatomic CoCrFeMnNi Cantor alloy is paramagnetic in a single Face-centered Cubic (FCC) phase at room temperature due to the severe anti-ferromagnetic coupling effect from Mn and Cr [26,27]. Thus, in this work, $Fe_{30}Co_{30}Ni_{30}Cr_{10-x}Mn_x$ high entropy alloys (x = 0, 5, 10 at.%) are investigated by systematically modified the ferromagnetic and anti-ferromagnetic elements. A mathematical model for CTE prediction of the materials under the influence of the Invar effect has also been established to demonstrate the mechanism of suppressed CTE behaviors in these HEAs systems. This research contributes to the understanding of the thermal expansion behaviors of Co–Cr–Fe–Mn–Ni HEAs and may provide a guideline to design future low CTE alloys for elevated temperature applications.

2. Experimental methods

2.1. Materials

For material preparation, FeCoNi and $Fe_{30}Co_{30}Ni_{30}Cr_{10-x}Mn_x$ (x = 0, 5, 10) were prepared by arc-melting pure elements with purity higher than 99.9% wt.% under a Ti-gettered and high purity argon atmosphere on a water-cooled copper mold. The alloys were re-melted five times and flipped each time to improve the chemical homogeneity and solution heat treatment at 1273 K for 20 h. The sample size after vacuum-arc melting was an oblate shape with a diameter around 35 mm and 50 g in weight. Since CTE of Invar alloys could be affected by heat treatments [7], all the samples were annealed under the same condition at 1123 K for 30 min, then quenched in water. The compositions of the samples were checked and confirmed by energy-dispersive X-ray spectroscopy (EDS, AZtec). ThermoCalc 2021 thermodynamic simulation software with TCHEA4 database was used to compute possible phase constituents in the alloys and phase identification was performed by X-ray diffractometer analysis (D2 PHASER X-ray diffractometer, BRUKER) equipped with Cu (Kα radiation = 1.5406 Å) target. Microstructural analysis on the specimens was performed by JEOL JSM-7610F with BSE detectors.

2.2. Thermal expansion analysis

For experimental CTE measurement, the test samples were machined from the heat-treated ingots into cylinders with 6 mm in diameter, 10 mm in height and ground the surface with #1200 sandpaper. Length change of samples was recorded from 400 K to 1200 K with 3 K per minute heating rate using thermal dilatometers (TMA 92 SETARAM) under high purity argon atmosphere to prevent the formation of the discontinuous and high CTE oxide layer, such as NiO and Fe_2O_3 (CTE~14.9–17.1 ppm/K) [28]. CTE was then derived from the rate of length change divided by temperature difference.

A mathematical model to predict CTE of the material under the influence of the Invar effect is proposed to examine the anomalous CTE properties of HEAs. The CTE of material is assumed to consist of two parameters: theoretical thermal lattice expansion α_T from the increasing level of thermal agitation and equilibrium vacancy concentration, and lattice contraction $\alpha_{shrinkage}$ by the Invar effect [3]. α_T, the CTE value without the influence of Invar effect, can be described by combining theories of Debye–Grüneisen relation [29] and Arrhenius equation of vacancy formation defined as $N\nu = \exp(-\Delta E/k_B T)$ [29,30]. The equations for calculating α_T of the alloys are listed as below and the deduction process is presented in **Appendix I**.

$$\alpha_T = \alpha_L \left(1 - e^{-T/\theta_D}\right)\left(1 - e^{-H^f/k_B T}\right) \tag{1}$$

$$\alpha_L = \gamma C_V / 3VK_T \tag{2}$$

$$C_V = 9Nk_B \left(T/\theta_D\right)^3 \int_0^{x_D} x^4 e^x/(e^x - 1)^2\, dx \tag{3}$$

Here, α_L is the coefficient of linear thermal expansion from lattice vibration, k_B is Boltzmann constant, K_T is the isothermal bulk modulus, C_V is the molar heat capacities at constant volume, V is molar volume, $\gamma$is Grüneisen constant, θ_D is the Debye temperature, x equals to $\theta_D/T$and N is the number of atoms per molar volume.

For calculation of lattice shrinkage $\alpha_{shrinkage}$ from Invar effect, a mathematical model has been established based on the Langevin theory of paramagnetism. The theory was developed by Langevin [31] and extended by Weiss [32] to include ferromagnetism and extrapolated in this research to model temperature-dependent magneto-crystalline anisotropy rotating behavior which describes the spontaneous volume magnetostriction of Invar alloys [2,33,34]. This model is used to derive the CTE value under the influence of the Invar effect $\alpha_{Invar\ effect}$ by subtracting shrinkage behavior $\alpha_{shrinkage}$ from the Invar effect with α_T. The relation between $\alpha_{Invar\ effect}$ and $\alpha_{shrinkage}$ is listed below and step-by-step deductions for $\alpha_{shrinkage}$ and $\alpha_{Invar\ effect}$ are presented in **Appendix II**.

$$\alpha_{Invar\ effect} = \alpha_T - \alpha_{shrinkage} \tag{4}$$

$$\alpha_{shrinkage} = \Delta l/\Delta T = A\Delta E/T\cdot\Delta T \tag{5}$$

Here, E is elastic modulus and A is a constant based on the magnetocrystalline anisotropy properties of the material with the Invar effect and can be derived by experimental CTE data.

2.3. Magnetic properties analysis

In order to determine the underlying mechanism of possible suppressed thermal expansion behavior of FeCoNi and $Fe_{30}Co_{30}Ni_{30}Cr_{10-x}Mn_x$, the magnetic properties were characterized by a Vibrating Sample Magnetometer (VSM 7410/J, LAKE SHORE) since the Invar effect is related to the ferromagnetism of the material [1,2,35,36]. Magnetic hysteresis loop (M − H), magnetic saturation magnetization (Ms), and coercive field (Hc) were measured with the VSM under magnetic field ranging from −5000 Oe to 5000 Oe. The magnetic moment as a function of temperature (M-T) was acquired by a High-temperature VSM (HTVSM). The samples were heated up from room temperature to 1150 K with an applied field of 3000 Oe under high purity argon atmosphere. Tc was determined by the maximum curvature method which Tc is the temperature where $|dM/dT|$ exhibits maximum value [37]. The magnetic entropy difference ΔS_m can be calculated from the M-T curves using Maxwell relation $\Delta S_m = \mu_0 \int_0^H \left(\partial M/\partial T\right)_H dH$ [38] and we integrated the total amount of ΔS_m ±50 K from Tc for the comparison effect of varying Mn and Cr.

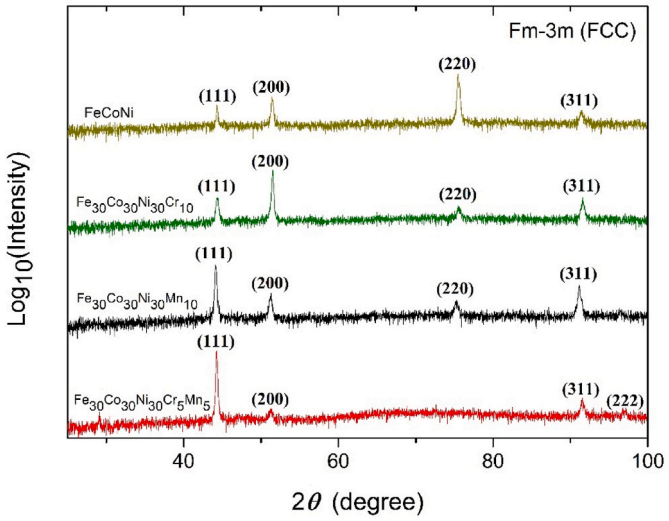

Fig. 1. X-ray diffraction profile (CuK_α) for FeCoNi and $Fe_{30}Co_{30}Ni_{30}Cr_{10-x}Mn_x$.

Table 1
Average lattice parameter of FCC FeCoNi and $Fe_{30}Co_{30}Ni_{30}Cr_{10-x}Mn_x$.

	Lattice parameter (298 K)
FeCoNi	3.5553 ± 0.0114 Å
$Fe_{30}Co_{30}Ni_{30}Cr_{10}$	3.5508 ± 0.0119 Å
$Fe_{30}Co_{30}Ni_{30}Mn_{10}$	3.5640 ± 0.0093 Å
$Fe_{30}Co_{30}Ni_{30}Cr_5Mn_5$	3.5572 ± 0.0087 Å
Invar 36 (FCC, ferromagnetic state)	3.592 Å [41]
$Fe_{65}Mn_{35}$ (FCC, anti-ferromagnetic state)	3.613 Å [42]

3. Results and analysis

3.1. Phase analysis

Results of the XRD patterns are present in Fig. 1. The XRD analysis indicates that, after heat treatment, FeCoNi and $Fe_{30}Co_{30}Ni_{30}Cr_{10-x}Mn_x$ (x = 0, 5, 10) alloys are mainly FCC phase structure which is the typical phase for low CTE Invar alloys [2]. The peak intensity of the XRD pattern varies due to grain texture difference from sampling, and texture would have minimal influence on CTE since the thermal expansion behavior of all the samples is isotropic. Table 1 lists the lattice parameters of FeCoNi and $Fe_{30}Co_{30}Ni_{30}Cr_{10-x}Mn_x$ derived from XRD peaks at room temperature. $Fe_{30}Co_{30}Ni_{30}Mn_{10}$ exhibits the highest lattice parameter while $Fe_{30}Co_{30}Ni_{30}Cr_{10}$ shows the lowest among $Fe_{30}Co_{30}Ni_{30}Cr_{10-x}Mn_x$. The higher lattice parameter of $Fe_{30}Co_{30}Ni_{30}Mn_{10}$ indicates the more positive exchange energy of transition metals and is expected to have more intense ferromagnetism based on the Bethe-Slater curve [39,40]. Furthermore, FeCoNi and $Fe_{30}Co_{30}Ni_{30}Cr_{10-x}Mn_x$ exhibit distinctively lower lattice parameters in contrast to the extremely low CTE Invar 36 alloy (FCC) and anti-ferromagnetic state $Fe_{65}Mn_{35}$ Invar alloy (FCC). This phenomenon may imply that atomic spacing may relate to the intensity of the Invar effect in FCC phase 3d transition metal alloys. Fig. 2 presents the SEM images (BEI) of FeCoNi and $Fe_{30}Co_{30}Ni_{30}Cr_{10-x}Mn_x$ alloys indicating the single FCC phase structure in all samples.

3.2. Coefficient of thermal expansion (CTE)

Fig. 3 presents the temperature dependence dL/L and CTE curve of FeCoNi, $Fe_{30}Co_{30}Ni_{30}Cr_{10-x}Mn_x$ and their average CTE in different temperature ranges are given in Table 2. CTE values up to 900 K of FeCoNi and $Fe_{30}Co_{30}Ni_{30}Cr_{10-x}Mn_x$ are 9.6–12.4 ppm/K comparing to that of CTE value of Cantor alloy (17–23 ppm/K, from 450 to 900 K) done by G. Laplanche et al. [43]. At a specific temperature region where second-order phase transition occurs, CTE of all the alloys raises

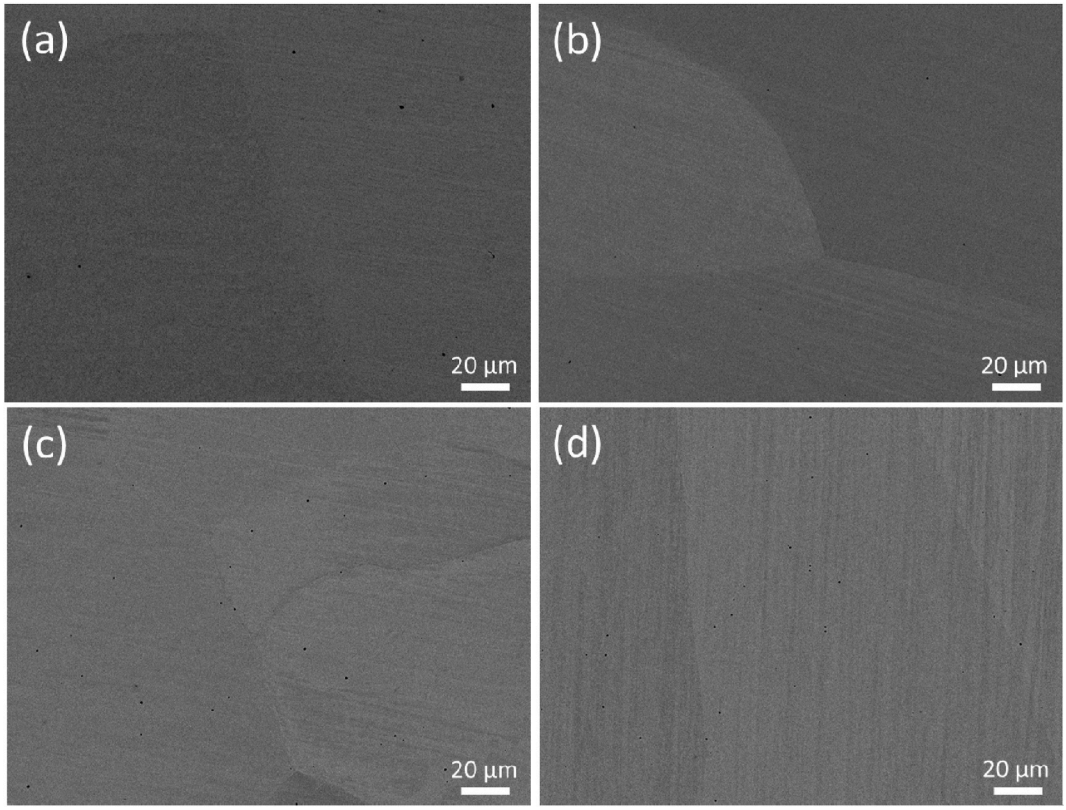

Fig. 2. SEM (BEI) images of (a) FeCoNi, (b) $Fe_{30}Co_{30}Ni_{30}Cr_{10}$, (c) $Fe_{30}Co_{30}Ni_{30}Mn_{10}$, and (d) $Fe_{30}Co_{30}Ni_{30}Cr_5Mn_5$.

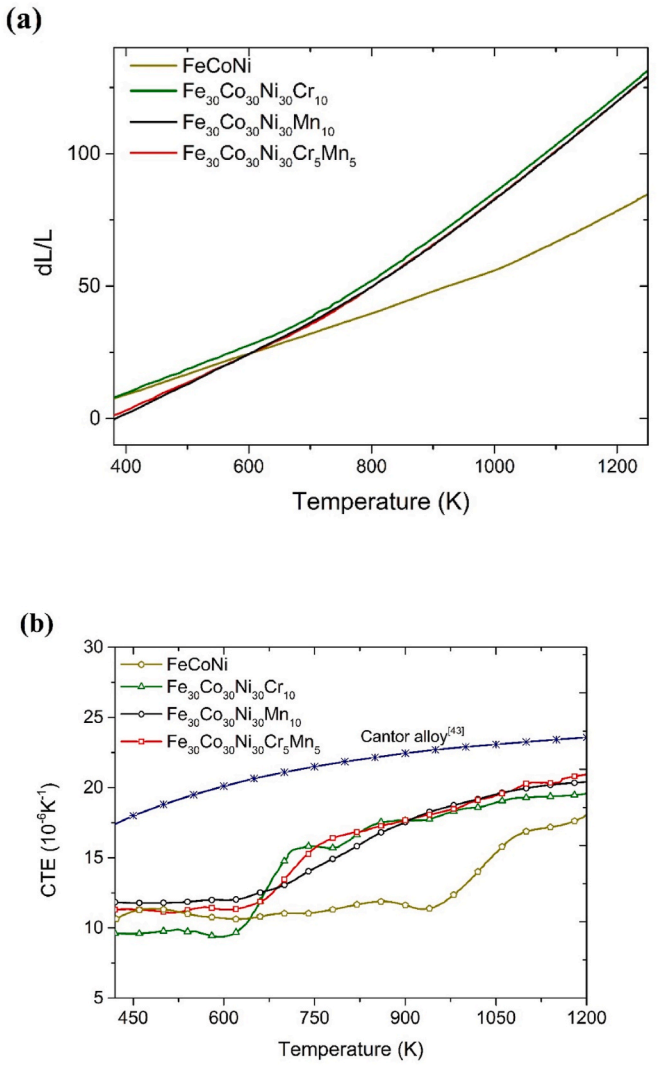

Fig. 3. Thermal expansion properties of FeCoNi and $Fe_{30}Co_{30}Ni_{30}Cr_{10-x}Mn_x$. (a) Linear thermal expansion dL/L. (b) Temperature dependence differential CTE curves.

significantly, and replacing Cr with Mn would increase the CTE transition temperature. At elevated temperatures, an increased level of equilibrium vacancy concentration would cause a slight CTE increase [3]. To confirm the mechanism of suppressed expansion behavior of the HEAs, magnetic properties are further examined.

3.3. Magnetic hysteresis loop ($M-H$) and temperature dependent magnetization curve (M-T)

The magnetic hysteresis loops were determined by VSM at room temperature. Fig. 4 shows the $M-H$ curves of FeCoNi and $Fe_{30}Co_{30}Ni_{30}Cr_{10-x}Mn_x$. FeCoNi has the highest Ms 163 emu/g among four samples at room temperature. Comparing with the Cantor alloy which is paramagnetic due to severe anti-ferromagnetic coupling effect from Mn and Cr [26], ferromagnetism of $Fe_{30}Co_{30}Ni_{30}Cr_{10-x}Mn_x$ is pronounced. Hc values of all samples are between 16 and 22 Oe indicating the soft ferromagnet property.

The temperature dependent magnetization curves were accurately determined by HTVSM under 3000 Oe applied field to measure Tc. Fig. 5 demonstrates the M-T curves of FeCoNi and $Fe_{30}Co_{30}Ni_{30}Cr_{10-x}Mn_x$. Tc of FeCoNi, $Fe_{30}Co_{30}Ni_{30}Cr_{10}$, $Fe_{30}Co_{30}Ni_{30}Cr_{10}$ and $Fe_{30}Co_{30}Ni_{30}Cr_5Mn_5$ is 1000 K, 651 K, 741 K and 696 K respectively. FeCoNi has the highest Tc due to the high intrinsic Tc value of the Co and the addition of Cr and Mn reduces Tc. For $Fe_{30}Co_{30}Ni_{30}Cr_{10-x}Mn_x$, replacing Cr with Mn raises Tc from 651 K to 741 K. The Tc difference between FeCoNi and $Fe_{30}Co_{30}Ni_{30}Cr_{10-x}Mn_x$ suggests the content of Cr or Mn within 10 at.% reduce Tc and Ms while still maintains the overall ferromagnetism at elevated temperature.

3.4. Calculation of α_T and $\alpha_{Invar\ effect}$

To further clarify the underlying mechanism of the suppressed CTE behavior, we calculated the CTE value with and without the Invar effect. In Table 3, we listed the parameters used to calculate α_T of FeCoNi and $Fe_{30}Co_{30}Ni_{30}Cr_{10-x}Mn_x$ from the Grüneisen relation and Debye model without the influence of the Invar effect.

For bulk modulus K_T, prior researches [33,45] generally treated the bulk modulus as a constant in the calculation of the Grüneisen relation. However, the bulk modulus of Invar alloys anomalously varies with temperature due to the Invar effect [46,47]. To eliminate the influence of Invar effect, paramagnetic state values of FeCoNi and $Fe_{30}Co_{30}Ni_{30}Cr_{10-x}Mn_x$ have been adopted in this work.

For γ and θ_D, we referenced the work by White [48] to set a standard θ_D for Invar alloys. Since lack of attainable data, γ and θ_D were determined by substituting the high temperature region of experimental CTE data to $\alpha_L = \gamma C_V/3VK_T$ (See (2) in **2.2**). We notice that the alloying effect on θ_D is related to bulk modulus. The composition with higher bulk

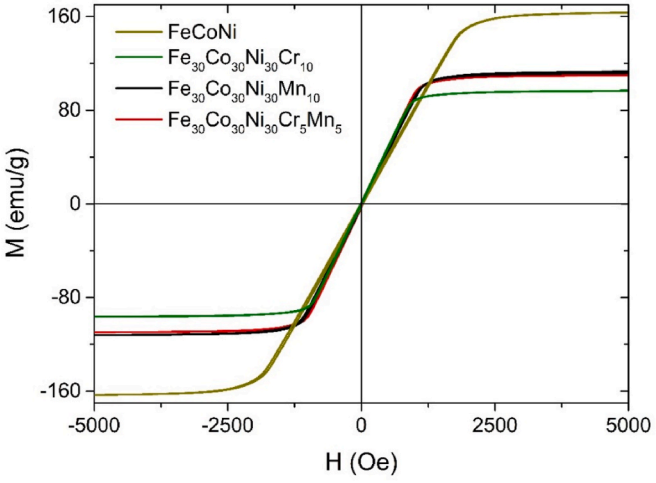

Fig. 4. Magnetic hysteresis loops of FeCoNi and $Fe_{30}Co_{30}Ni_{30}Cr_{10-x}Mn_x$ from ±5000 Oe applied magnetic field at room temperature.

Table 2
Average CTE values of FeCoNi and $Fe_{30}Co_{30}Ni_{30}Cr_{10-x}Mn_x$.

CTE (10^{-6}/K)	Temperature (K)					
	420–470	620–670	670–720	720–770	965–1015	1100–1150
FeCoNi	11.08	10.71	11.00	11.09	12.75	17.08
$Fe_{30}Co_{30}Ni_{30}Cr_{10}$	9.59	10.96	14.43	15.77	18.40	19.34
$Fe_{30}Co_{30}Ni_{30}Mn_{10}$	11.86	12.10	13.12	14.03	18.94	20.24
$Fe_{30}Co_{30}Ni_{30}Cr_5Mn_5$	11.31	11.63	13.17	15.43	18.63	20.34

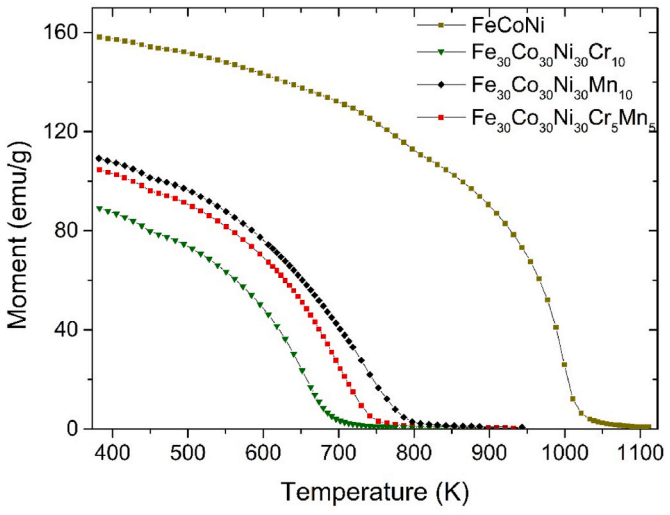

Fig. 5. Temperature dependent magnetization curves of FeCoNi and $Fe_{30}Co_{30}Ni_{30}Cr_{10-x}Mn_x$ in 3000 Oe applied magnetic field.

Table 3
Calculation parameters of α_T on FeCoNi and $Fe_{30}Co_{30}Ni_{30}Cr_{10-x}Mn_x$.

	K_T (N/m^2)	V (cm^3)	γ	θ_D (K)	H^f (ev)
FeCoNi	1.742×10^{11} [44]	6.88	1.63	368	1.53
$Fe_{30}Co_{30}Ni_{30}Cr_5Mn_5$	1.74×10^{11} [44]	6.82	2.19	400	1.56
$Fe_{30}Co_{30}Ni_{30}Cr_{10}$	1.87×10^{11} [44]	6.80	2.85	415	1.59
$Fe_{30}Co_{30}Ni_{30}Mn_{10}$	1.47×10^{11} [44]	6.84	2.45	380	1.53

modulus tends to exhibit larger θ_D [49] and we use this effect to examine the validity of the derived θ_D. For H^f value, each composition was calculated with atomic ratio multiplying by the value of pure element vacancy formation enthalpy [50]; the result is within error with respect to first-principles calculations [51–53]. By substituting all the parameters into the mathematical model, we calculated α_T for all alloys in different temperature region. To examine the anomalous CTE behavior of FeCoNi and $Fe_{30}Co_{30}Ni_{30}Cr_{10-x}Mn_x$, α_T and $\alpha_{Invar\ effect}$ were derived around their Tc. In the mathematical model of $\alpha_{Invar\ effect}$, constant A and Young's modulus E of each alloy were calculated from the experimental CTE results and the reported data [24,43,54]. Using α_T and $\alpha_{Invar\ effect}$ to plot the calculated CTE curves and experimental CTE data around Tc yields the dash line and dot-dash line in Fig. 6; the solid line is experimental data.

3.5. Magnetic entropy difference

ΔS_m was measured to enlighten the correlation between the configurational entropy and the magnetic entropy in the HEA system. Temperature dependent ΔS_m curves of the FeCoNi and $Fe_{30}Co_{30}Ni_{30}Cr_{10-x}Mn_x$ were measured with 3000 Oe field which is enough to fully magnetized the samples according to the M − H curve and were derived from M-T curves by using Maxwell relation: $\Delta S_m = \mu_0 \int_0^H \left(\partial M/\partial T\right)_H dH$ and their results are presented collectively in Fig. 7. To examine the effect of replacing Cr with Mn to magnetic entropy difference, we integrated $|\Delta S_m|$ curve ±50 K from the Tc and the results are presented in Table 4. The sum of $|\Delta S_m|$ of FeCoNi is around 150% higher than $Fe_{30}Co_{30}Ni_{30}Cr_{10-x}Mn_x$ due to the intense ferromagnetism. Among $Fe_{30}Co_{30}Ni_{30}Cr_{10-x}Mn_x$, the highest configurational entropy $Fe_{30}Co_{30}Ni_{30}Cr_5Mn_5$ also exhibits the highest total $|\Delta S_m|$.

4. Discussion

Using the $Fe_{64}Ni_{36}$ Invar 36 alloy, a well-known single FCC phase alloy with extremely low CTE, as the starting composition, CALPHAD prediction (Fig. 8) indicates that the large FCC phase field can be extended to FeCoNi and $Fe_{30}Co_{30}Ni_{30}Cr_{10-x}Mn_x$ HEAs and would undergo a magnetic second-order phase transition at elevated temperature; although FCC phase decomposition could occur according to the phase diagram, FCC phase was maintained in all alloys by fast quenching process in this work. The red dash line shows the predicted Tc by Thermo-Calc; Tc of Invar 36 would increase when Fe and Ni are substituted with Co and significantly decrease when Mn and Cr are enriched, this trend is consistent with the HTVSM results shown in Fig. 5, but the measured Tc value by experiments and the predicted Tc values do not match. This difference may be due to the fact that the Invar effect was not yet considered in the TCHEA4 database for Thermo-Calc prediction.

The CTE behaviors of HEAs in Fig. 3 can be divided into three temperature regions: temperature below Tc (ferromagnetic), Tc transition region (ferromagnetic to paramagnetic), and temperature above Tc (paramagnetic). When the temperature is below Tc, the experimental CTE of FeCoNi and $Fe_{30}Co_{30}Ni_{30}Cr_{10-x}Mn_x$ are all lower than α_T demonstrating the dimensionally stable properties of the HEAs (See the dash line in Fig. 6). In contrast to that of equal molar Cantor alloy, CTE values of $Fe_{30}Co_{30}Ni_{30}Cr_{10-x}Mn_x$ are significantly lowered by 45.2%. The range of difference between the experimental CTE values of FeCoNi and $Fe_{30}Co_{30}Ni_{30}Cr_{10-x}Mn_x$ from 620 to 670 K and α_T is 14.8–29.5% (FeCoNi = 29.5%, $Fe_{30}Co_{30}Ni_{30}Cr_{10}$ = 26.7%, $Fe_{30}Co_{30}Ni_{30}Cr_5Mn_5$ = 23.8%, $Fe_{30}Co_{30}Ni_{30}Mn_{10}$ = 14.8%), and the discrepancy arises from different level of Invar effects in each alloy system. In Table 2, average CTE values of $Fe_{30}Co_{30}Ni_{30}Cr_{10-x}Mn_x$ between 420 and 470 K are 9.59–11.86 ppm/K which only exhibit a slight difference in contrast to the CTE value of FeCoNi (11.08 ppm/K), indicating that the addition of anti-ferromagnetic elements does not significantly raise the CTE below Tc. The trend is very different from the commercial Invar alloys which their CTE would be greatly increased with the addition of anti-ferromagnetic elements [2,34]. This phenomenon may cause by the valence electron concentration (e/a) of the $Fe_{30}Co_{30}Ni_{30}Cr_{10-x}Mn_x$. For ferromagnetic/anti-ferromagnetic state Invar alloy systems including Fe–Ni, Fe–Mn, Fe–Pt, Mn–Co, Fe–Ni–Mn, Fe–Ni–Cr, Fe–Cr–Mn, and Fe–Ni–Co alloys, there exists two minima CTE (at 298 K) value in ferromagnetic range e/a = 8.5–8.7 and the antiferromagnetic range around e/a = 7.6 [55–57]; CTE exhibits maxima value when e/a = 8.3 (in the spin-glass range) where the CTE of the Invar alloys is larger than pure copper [2]. For FeCoNi, $Fe_{30}Co_{30}Ni_{30}Cr_{10-x}Mn_x$ and CoCrFeMnNi Cantor alloy, the e/a values are 9.0, 8.7–8.9 and 8.0 respectively. This study found that the CTE results of HEA systems also align with the e/a tendency of Invar alloy systems as the CTE of the Cantor alloy (17–22 ppm/K, e/a = 8.0) is significantly higher than the CTE of FeCoNi and $Fe_{30}Co_{30}Ni_{30}Cr_{10-x}Mn_x$ (9.5–11.6 ppm/K, e/a = 8.7–9.0). Thus, if we decrease Cr and Mn from Cantor alloy to FeCoNi, the CTE value of the HEA is expected to slightly increase (until e/a = 8.3, max. CTE) followed by a distinctive decrease in CTE (until e/a = 8.5–8.7, min. CTE) and finally increases again. The experimental CTE of $Fe_{30}Co_{30}Ni_{30}Cr_{10}$ exhibits the lowest value among FeCoNi and $Fe_{30}Co_{30}Ni_{30}Cr_{10-x}Mn_x$ alloys before Tc as the e/a value of $Fe_{30}Co_{30}Ni_{30}Cr_{10}$ equals 8.7 which indicates the most intense Invar effect in contrast to other HEAs. $Fe_{30}Co_{30}Ni_{30}Mn_{10}$ shows a similar CTE value to FeCoNi; however, the e/a value of $Fe_{30}Co_{30}Ni_{30}Mn_{10}$ is closer to 8.7 than FeCoNi. This phenomenon implies that despite the $Fe_{30}Co_{30}Ni_{30}Mn_{10}$ exhibits more intense Invar effect than FeCoNi (e/a difference is 0.1), the intrinsic CTE value of each element will still take part in the determination of CTE of the HEA as pure Mn exhibits a much higher CTE value (~21.7 ppm/K) than Fe, Co, and Ni (~13 ppm/K). Thus, this research confirms that the tendency of low CTE e/a value for Invar alloy systems can be applied to HEA systems while the intrinsic CTE value of each component is also a

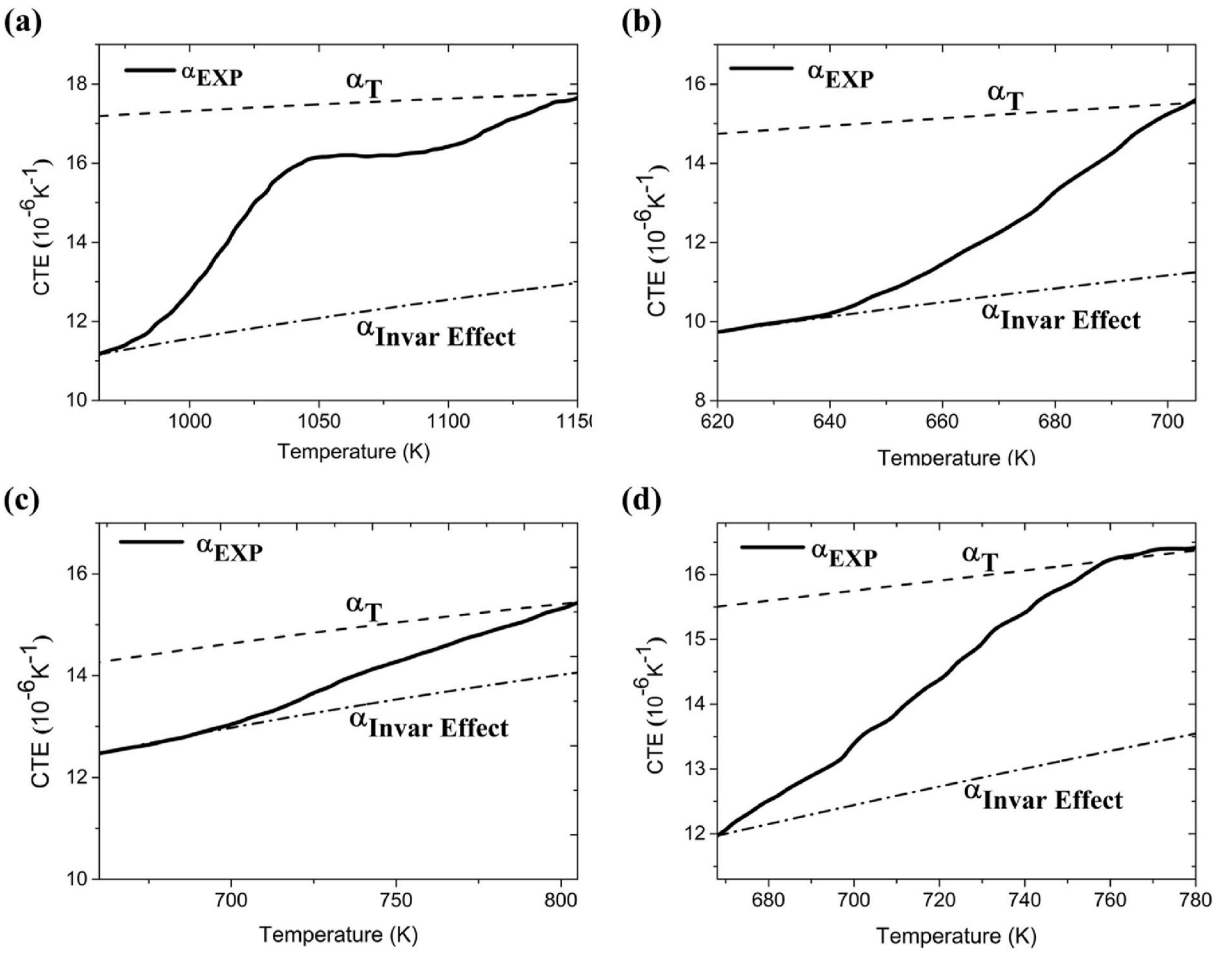

Fig. 6. Experimental and calculated temperature dependent CTE curves from the mathematical model around Tc. The dash line is α_T, the calculated CTE value without Invar effect; dot-dash line is $\alpha_{Invar\ effect}$, the calculated CTE under the influence of Invar effect, and the solid line is experimental data. (a) FeCoNi (b) $Fe_{30}Co_{30}Ni_{30}Cr_{10}$ (c) $Fe_{30}Co_{30}Ni_{30}Mn_{10}$ (d) $Fe_{30}Co_{30}Ni_{30}Cr_5Mn_5$.

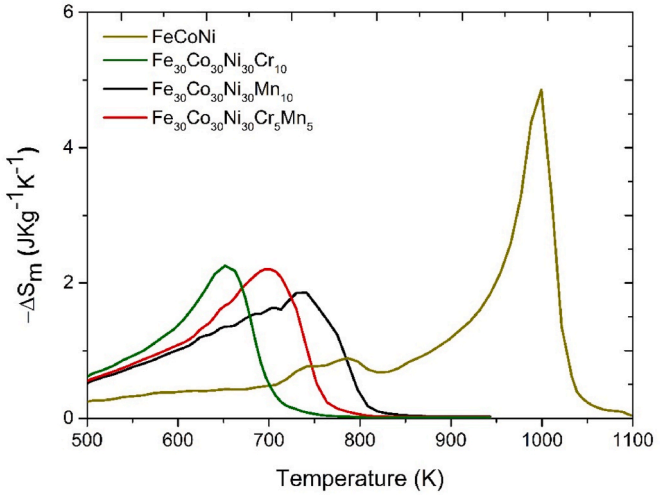

Fig. 7. Temperature dependent magnetic entropy change ΔS_m of FeCoNi and $Fe_{30}Co_{30}Ni_{30}Cr_{10-x}Mn_x$ with 3000 Oe magnetic field.

crucial factor.

In the Tc transition region, the thermal agitation significantly affects the magnetic coupling and triggers the ferromagnetism to paramagnetism transition causing experimental CTE to deviate from $\alpha_{Invar\ effect}$ and α_T (See Fig. 6). In the HEA system, it is noted that the addition of Cr and Mn would considerably reduce the Tc transition region. For FeCoNi composing only ferromagnetic elements, the transition region is around 180 K; for $Fe_{30}Co_{30}Ni_{30}Cr_{10-x}Mn_x$ HEAs, the Tc transition region is between 60 and 100 K.

When the temperature is above Tc, suppressed CTE phenomenon gradually fades as the alloy becomes paramagnetic, and CTE increase can be observed due to the elevating vacancy numbers. In Fig. 3, the CTE values of $Fe_{30}Co_{30}Ni_{30}Cr_{10-x}Mn_x$ above 1150 K are between 19 and 20 ppm/K while CTE of FeCoNi is around 18 ppm/K. This CTE difference between FeCoNi and $Fe_{30}Co_{30}Ni_{30}Cr_{10-x}Mn_x$ is likely originated from the different equilibrium vacancy concentration at the elevated temperature where no Invar effect exists. As the number of vacancies is the main contribution of the CTE increase at high temperatures, $Fe_{30}Co_{30}Ni_{30}Cr_{10-x}Mn_x$ would possibly exhibit lower vacancy activation energy than that of FeCoNi due to its higher CTE value. This phenomenon lines up with the study in which the vacancy activation energy of equal molar CoCrFeMnNi (2.78 ± 0.08eV) is lower than most of its composed pure elements Fe, Co, Ni, and Cr (2.95 eV–3.2 eV) [58]. The CTE transition temperature for the alloys in this work overlaps with Tc value from HTVSM results. As experimental CTE values are significantly lower than α_T calculation and the CTE transition temperature overlaps with Tc, it can be deduced that the Invar effect does exist in $Fe_{30}Co_{30}Ni_{30}Cr_{10-x}Mn_x$ HEAs with high Cr contents and causes the suppressed CTE behavior.

The M-T curve (Fig. 5) shows that, around Tc, FeCoNi exhibits a distinct decrease of ferromagnetism with increasing temperature, while ferromagnetism of $Fe_{30}Co_{30}Ni_{30}Cr_{10-x}Mn_x$ drops slowly with elevating

Table 4
Sum of $|\Delta S_m|$ ±50 K from the Tc of FeCoNi and $Fe_{30}Co_{30}Ni_{30}Cr_{10-x}Mn_x$.

JKg^{-1}	FeCoNi	$Fe_{30}Co_{30}Ni_{30}Mn_{10}$	$Fe_{30}Co_{30}Ni_{30}Cr_5Mn_5$	$Fe_{30}Co_{30}Ni_{30}Cr_{10}$
$\|\Delta S_m\|$	264.239	158.681	179.189	173.185
(±50 K from Tc)	(950–1050 K)	(691–791 K)	(649–749 K)	(601–701 K)

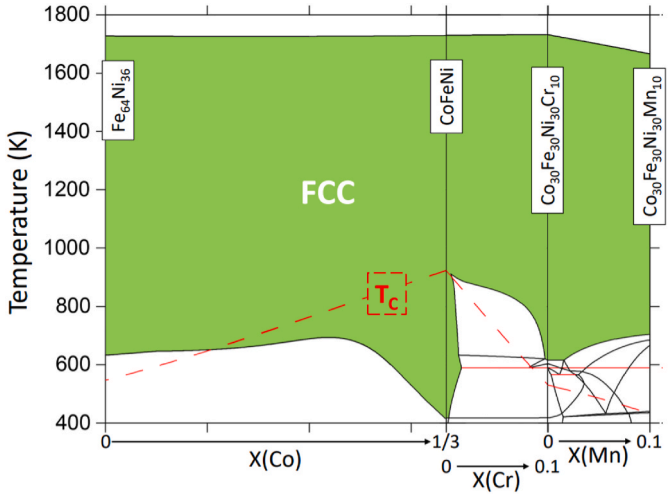

Fig. 8. Thermo-Calc simulation phase diagram and calculated Tc in single FCC phase on $Fe_{64}Ni_{36}$ (Invar 36), FeCoNi and $Fe_{30}Co_{30}Ni_{30}Cr_{10-x}Mn_x$.

temperature. This phenomenon is likely caused by the spin glass properties of Cantor alloy [26] from the mixing of ferromagnetic and anti-ferromagnetic elements. Addition of total 10 at.% Cr and Mn to FeCoNi can decrease Ms from 163 emu/g to between 96 and 113 emu/g and also drop the Tc from 1000 K to 651 K. Replacing Cr with Mn increases Ms and Tc, indicating that Cr can provide a more intense anti-ferromagnetic coupling effect than that of Mn in the $Fe_{30}Co_{30}Ni_{30}Cr_{10-x}Mn_x$ system. It should be noted that the ferromagnetic state aligns with the $\alpha_{Invar\ Effect}$ and the paramagnetic state matches the α_T since the suppressed CTE Invar effect exists only when the material is ferromagnetic [1,2,35,36]. We can thus derive the intrinsic transition of ferromagnetism to paramagnetism by the experimental CTE data around Tc without an applied magnetic field. The relation can be written as below, where $\alpha_{measured}$ is the measured CTE value around Tc and X is the amount of ferromagnetism.

$$\alpha_{measured} = X\alpha_{Invar\ Effect} + (1 - X)\alpha_T \quad (6)$$

Previous studies report that measuring Tc with the applied magnetic field may cause deviation due to the susceptibility difference from spontaneous magnetization, rotation of anisotropy, domain wall motion, and superparamagnetism if field intensity is not selected properly [37,59,60]. This procedure may pioneer a new method to obtain ferromagnetic properties by using the temperature dependent CTE curve and offers a new approach for future researches on the intrinsic properties of magnetic materials.

In Fig. 7, the maximum ΔS_m of $Fe_{30}Co_{30}Ni_{30}Cr_{10-x}Mn_x$ under 3000 Oe applied field (−1.85 to −2.24 $JKg^{-1}K^{-1}$, with decreasing x) are 6 times higher than the reference cold-rolled FeCoCrNi HEAs (−0.35 $JKg^{-1}K^{-1}$) in 20,000 Oe applied field [61]. For the sum of the ΔS_m ±50 K from Tc, it is particularly noted that the highest configurational entropy sample $Fe_{30}Co_{30}Ni_{30}Cr_5Mn_5$ exhibits the highest magnetic entropy difference in $Fe_{30}Co_{30}Ni_{30}Cr_{10-x}Mn_x$. The origin of this phenomenon is likely associated with the effect of Tc and Ms of the HEAs. Tc determines the temperature range for deducting magnetic entropy difference. At high temperature, severe thermal agitation could interact with the spin-coupling in the ferromagnetic state, resulting in the decrease of the magnetic ordering. Ms can determine the level of magnetic ordering [38] and the high level of Ms contributes to a large entropy difference between the magnetic order state and thermally disorder state. The large difference between the sum of $|\Delta S_m|$ FeCoNi (264.23 JKg^{-1}, Ms equals 158 emu/g at 400 K) and $Fe_{30}Co_{30}Ni_{30}Cr_{10}$ (173.18 JKg^{-1}, Ms equals 89 emu/g at 400 K) confirms this effect. Thus, for $Fe_{30}Co_{30}Ni_{30}Cr_{10-x}Mn_x$ HEAs, Cr addition could decrease Tc, leading to the rise of the magnetic entropy change, while Cr could also reduce Ms of the alloy and decrease the magnetic entropy difference. Hence, the counteracting effect of Tc and Ms of Cr addition results in the highest configurational entropy alloy to possess the highest ΔS_m.

To the best of the authors' knowledge, this work is the first to report the Invar effect of suppressed CTE phenomena in HEAs. By modifying the antiferromagnetic elements of Cantor alloy within 10 at.%, both the ferromagnetism and Tc are significantly enhanced, and the effect can lead to the emergence of the suppressed CTE behavior due to the Invar effect. The experimental results confirm that the Invar effect can exist in the HEA system and the addition of anti-ferromagnetic elements does not significantly influence the CTE behavior before reaching Tc. This discovery offers a new strategy to develop high temperature, high dimensionally stable alloys, with an aim to raise the Cr ratio in order to avoid a possible debit of losing oxidation resistance at elevated temperatures.

5. Conclusion

This work demonstrates that decrease in thermal expansion can be caused by limiting the amount of Cr and Mn in the Co–Cr–Fe–Mn–Ni HEA system, and has confirmed the Invar effect to be the underlying mechanism, which is related to ferromagnetic properties of $Fe_{30}Co_{30}Ni_{30}Cr_{10-x}Mn_x$. Key findings are listed as follows.

1. An abrupt change of thermal expansion behavior related to the transition from ferromagnetism to paramagnetism could be observed in $Fe_{30}Co_{30}Ni_{30}Cr_{10-x}Mn_x$ HEAs. Replacing Mn with Cr leads to a decrease in both CTE value and CTE transition temperature due to the decrease of e/a value.
2. As demonstrated by experiments and theoretical thermal expansion calculation, we confirmed the suppressed CTE behavior of $Fe_{30}Co_{30}Ni_{30}Cr_{10-x}Mn_x$ is originated from the Invar effect even with the high concentration of antiferromagnetic elements present in the system.
3. Addition of total 10 at.% Cr and Mn to FeCoNi can decrease Ms from 163 emu/g to between 96 and 113 emu/g and also drop the Tc from 1000 K to between 651 K and 741 K. Replacing Cr with Mn increases the Ms and Tc, indicating that Cr has a more intense anti-ferromagnetic coupling effect than that of Mn in the $Fe_{30}Co_{30}Ni_{30}Cr_{10-x}Mn_x$ HEA system.
4. For $Fe_{30}Co_{30}Ni_{30}Cr_{10-x}Mn_x$, the maximum ΔS_m with 3000 Oe applied field is between −1.85 and −2.24 $JKg^{-1}K^{-1}$ and it is significantly higher than other similar HEA systems. The ΔS_m value becomes more negative when the x value decreases. The highest configurational entropy alloy, $Fe_{30}Co_{30}Ni_{30}Cr_5Mn_5$, also exhibits the largest sum of ΔS_m.
5. This work provides an understanding of the suppressed CTE phenomena in HEAs and offers a possibility for the development of high temperature high dimensionally stable materials in the future.

CRediT authorship contribution statement

Chun-Lin Lin: Formal analysis, Methodology, Investigation, Writing – original draft, Writing – review & editing. **Jhuo-Lun Lee:** Formal analysis, Methodology, Investigation, Writing – original draft, Writing – review & editing. **Shih-Ming Kuo:** Project administration, Supervision. **Ming-Yen Li:** Project administration, Supervision. **Lu Gan:** Formal analysis, Investigation. **Hideyuki Murakami:** Formal analysis, Investigation, Funding acquisition, Supervision. **Seiji Mitani:** Formal analysis, Investigation, Supervision. **Stéphane Gorsse:** Formal analysis, Investigation. **An-Chou Yeh:** Conceptualization, Methodology, Investigation, Writing – original draft, Writing – review & editing, Funding acquisition, Project administration, Supervision.

Declaration of competing interest

The authors declare that they have no known competing financial interests or personal relationships that could have appeared to influence the work reported in this paper.

Acknowledgement

Authors would like to thank the financial and material supports from China Steel Corporation (Proposal No. RE105620). Chun-Lin Lin would like to thank NIMS for the provision of the international collaborative graduate program (ICGP) scholarship. This work is supported by NIMS under the International Cooperative Graduate Program, and Ministry of Science and Technology (MOST) in Taiwan under Grant MOST110-2221-E-007-020-MY3, MOST110-2224-E-007 -001, and MOST109-2634-F-007-024; the "High Entropy Materials Center" from The Featured Areas Research Center Program within the framework of the Higher Education Sprout Project by the Ministry of Education.

Appendix A. Supplementary data

Supplementary data to this article can be found online at https://doi.org/10.1016/j.matchemphys.2021.124907.

References

[1] R. Roy, D.K. Agrawal, H.A. McKinstry, Very low thermal expansion coefficient materials, Annu. Rev. Mater. Sci. 19 (1) (1989) 59–81.
[2] E. Wasserman, Invar: moment-volume instabilities in transition metals and alloys, Handb. Ferromagn. Mater. 5 (1990) 237–322.
[3] E.H. Megchiche, C. Mijoule, M. Amarouche, First principles calculations of vacancy–vacancy interactions in nickel: thermal expansion effects, J. Phys. Condens. Matter 22 (48) (2010) 485502.
[4] A.A. Quong, A.Y. Liu, First-principles calculations of the thermal expansion of metals, Phys. Rev. B 56 (13) (1997) 7767.
[5] J. Elmer, D. Olson, D. Matlock, Thermal expansion characteristics of stainless steel weld metal, WELDING J 61 (9) (1982) 293.
[6] C.É. Guillaume, Recherches sur les aciers au nickel. Dilatations aux temperatures elevees; resistance electrique, C. R. Acad. Sci. 125 (235) (1897) 18.
[7] D.A.J.R. Davis, ASM Specialty Handbook: Nickel, Cobalt, and Their Alloys, ASM International Materials Park, OH, 2000, pp. 96–100.
[8] M. van Schilfgaarde, I. Abrikosov, B. Johansson, Origin of the Invar effect in iron–nickel alloys, Nature 400 (6739) (1999) 46.
[9] K. Sato, T. Ohno, Development of low thermal expansion superalloy, J. Mater. Eng. Perform. 2 (4) (1993) 511–516.
[10] E. Wanner, Development of a new controlled thermal expansion superalloy with improved oxidation resistance, Superalloys 1992 (1992) 237–246.
[11] R. Frank, The long-term thermal stability of thermo-span alloy, JOM 52 (1) (2000) 37–39.
[12] M.J. Donachie, S.J. Donachie, Superalloys: a Technical Guide, ASM international2002.
[13] J.H. Zhu, S. Geng, D. Ballard, Evaluation of several low thermal expansion Fe–Co–Ni alloys as interconnect for reduced-temperature solid oxide fuel cell, Int. J. Hydrogen Energy 32 (16) (2007) 3682–3688.
[14] Y.-T. Chen, Y.-J. Chang, H. Murakami, T. Sasaki, K. Hono, C.-W. Li, K. Kakehi, J.-W. Yeh, A.-C. Yeh, Hierarchical microstructure strengthening in a single crystal high entropy superalloy, Sci. Rep. 10 (1) (2020) 1–11.
[15] S. Gorsse, Y.-T. Chen, W.-C. Hsu, H. Murakami, A.-C. Yeh, Modeling the precipitation processes and the formation of hierarchical microstructures in a single crystal high entropy superalloy, Scripta Mater. 193 (2021) 147–152.
[16] T.-N. Lam, S.Y. Lee, N.-T. Tsou, H.-S. Chou, B.-H. Lai, Y.-J. Chang, R. Feng, T. Kawasaki, S. Harjo, P.K. Liaw, Enhancement of fatigue resistance by overload-induced deformation twinning in a CoCrFeMnNi high-entropy alloy, Acta Mater. 201 (2020) 412–424.
[17] D. Kumar, B. Jaishri, D.K. Meena, E.-W. Huang, Y.-J. Chang, A.-C. Yeh, J. Jain, S. Neelakantan, N.N. Gosvami, Reversal of favorable microstructure under plastic ploughing vs. interfacial shear induced wear in aged Co1. 5CrFeNi1. 5Ti0. 5 high-entropy alloy, Wear 468 (2021) 203595.
[18] T. Saito, A. Ishida, M. Yuyama, Y. Takata, K. Kawagishi, A.-C. Yeh, H. Murakami, Tensile creep behavior of single-crystal high-entropy superalloy at intermediate temperature, Crystals 11 (1) (2021) 28.
[19] Y.-T. Chen, Y.-J. Chang, H. Murakami, S. Gorsse, A.-C. Yeh, Designing high entropy superalloys for elevated temperature application, Scripta Mater. 187 (2020) 177–182.
[20] K.-C. Lo, H. Murakami, J.-W. Yeh, A.-C. Yeh, Oxidation behaviour of a novel refractory high entropy alloy at elevated temperatures, Intermetallics 119 (2020) 106711.
[21] Z. Rao, B. Dutta, F. Körmann, W. Lu, X. Zhou, C. Liu, A.K. da Silva, U. Wiedwald, M. Spasova, M. Farle, Beyond solid solution high-entropy alloys: tailoring magnetic properties via spinodal decomposition, Adv. Funct. Mater. 31 (7) (2021) 2007668.
[22] H.-P. Chou, Y.-S. Chang, S.-K. Chen, J.-W. Yeh, Microstructure, thermophysical and electrical properties in AlxCoCrFeNi ($0 \leq x \leq 2$) high-entropy alloys, Mater. Sci. Eng., B 163 (3) (2009) 184–189.
[23] L. Liu, S. Huang, L. Vitos, M. Dong, E. Bykova, D. Zhang, B.S. Almqvist, S. Ivanov, J.-E. Rubensson, B. Varga, Pressure-induced magnetovolume effect in CoCrFeAl high-entropy alloy, Commun. Phys. 2 (1) (2019) 1–9.
[24] G. Laplanche, P. Gadaud, C. Bärsch, K. Demtröder, C. Reinhart, J. Schreuer, E. P. George, Elastic moduli and thermal expansion coefficients of medium-entropy subsystems of the CrMnFeCoNi high-entropy alloy, J. Alloys Compd. 746 (2018) 244–255.
[25] Z. Rao, D. Ponge, F. Körmann, Y. Ikeda, O. Schneeweiss, M. Friák, J. Neugebauer, D. Raabe, Z. Li, Invar effects in FeNiCo medium entropy alloys: from an Invar treasure map to alloy design, Intermetallics 111 (2019) 106520.
[26] O. Schneeweiss, M. Friák, M. Dudová, D. Holec, M. Šob, D. Kriegner, V. Holý, P. Beran, E.P. George, J. Neugebauer, Magnetic properties of the CrMnFeCoNi high-entropy alloy, Phys. Rev. B 96 (1) (2017), 014437.
[27] P. Yu, L. Zhang, H. Cheng, H. Zhang, M. Ma, Y. Li, G. Li, P. Liaw, R. Liu, The high-entropy alloys with high hardness and soft magnetic property prepared by mechanical alloying and high-pressure sintering, Intermetallics 70 (2016) 82–87.
[28] M.F. Hasanabadi, A. Kokabi, A. Nemati, S.Z. Ajabshir, Interactions near the triple-phase boundaries metal/glass/air in planar solid oxide fuel cells, Int. J. Hydrogen Energy 42 (8) (2017) 5306–5314.
[29] E. Grüneisen, Theorie des festen Zustandes einatomiger Elemente, Ann. Phys. 344 (12) (1912) 257–306.
[30] R. Siegel, Vacancy concentrations in metals, J. Nucl. Mater. 69 (1978) 117–146.
[31] P. Langevin, Sur la théorie du magnétisme, 1905.
[32] P. Weiss, L'hypothèse du champ moléculaire et la propriété ferromagnétique, 1907.
[33] M. Matsui, S. Chikazumi, Analysis of anomalous thermal expansion coefficient of Fe–Ni Invar alloys, J. Phys. Soc. Jpn. 45 (2) (1978) 458–465.
[34] H. Ahluwalia, ASM specialty handbook: nickel, cobalt, and their alloys, Corrosion 58 (4) (2002) 381.
[35] S. Chikazumi, Invar anomalies, J. Magn. Magn Mater. 10 (Issues 2–3) (1979) 113–119.
[36] Y. Endoh, Y. Noda, Zero sound anomaly in a ferromagnetic invar alloy Fe65Ni35, J. Phys. Soc. Jpn. 46 (3) (1979) 806–814.
[37] K. Fabian, V.P. Shcherbakov, S.A. McEnroe, Measuring the Curie temperature, G-cubed 14 (4) (2013) 947–961.
[38] J.R. Gómez, R.F. Garcia, A.D.M. Catoira, M.R. Gómez, Magnetocaloric effect: a review of the thermodynamic cycles in magnetic refrigeration, Renew. Sustain. Energy Rev. 17 (2013) 74–82.
[39] N.W. Ashcroft, N.D. Mermin, Solid State Physics, holt, rinehart and winston, new york London, 1976.
[40] J.C. Slater, Cohesion in monovalent metals, Phys. Rev. 35 (5) (1930) 509.
[41] P. Gorria, D. Martínez-Blanco, M.J. Pérez, J.A. Blanco, A. Hernando, M.A. Laguna-Marco, D. Haskel, N. Souza-Neto, R.I. Smith, W.G. Marshall, Stress-induced large Curie temperature enhancement in Fe 64 Ni 36 Invar alloy, Phys. Rev. B 80 (6) (2009), 064421.
[42] P. Marinelli, M. Sade, A. Baruj, A.F. Guillermet, Lattice parameters of metastable structures in quenched Fe-Mn alloys. Pt. I. Experimental techniques, bcc and fcc phases, Zeitschrift für Metallkunde 91 (11) (2000) 957–962.
[43] G. Laplanche, P. Gadaud, O. Horst, F. Otto, G. Eggeler, E. George, Temperature dependencies of the elastic moduli and thermal expansion coefficient of an equiatomic, single-phase CoCrFeMnNi high-entropy alloy, J. Alloys Compd. 623 (2015) 348–353.
[44] H. Ge, H. Song, J. Shen, F. Tian, Effect of alloying on the thermal-elastic properties of 3d high-entropy alloys, Mater. Chem. Phys. 210 (2018) 320–326.
[45] S. Chikazumi, Invar anomalies, J. Magn. Magn Mater. 10 (2–3) (1979) 113–119.
[46] E. Török, G. Hausch, Bulk modulus anomaly of Fe-Ni and Fe-Pt invar alloys, Phys. Status Solidi 53 (2) (1979) K147–K151.
[47] G. Oomi, N. Mōri, Bulk modulus anomalies of Fe-Ni and Fe-Pt Invar alloys, J. Phys. Soc. Jpn. 50 (9) (1981) 2917–2923.
[48] G. White, Thermal expansion of magnetic metals at low temperatures, Proc. Phys. Soc. 86 (1) (1965) 159.

[49] S. Huang, Á. Vida, A. Heczel, E. Holmström, L. Vitos, Thermal expansion, elastic and magnetic properties of FeCoNiCu-based high-entropy alloys using first-principle theory, JOM (J. Occup. Med.) 69 (11) (2017) 2107–2112.
[50] T. Abe, Thermal Vacancies in High-Entropy Alloys, MATERIALS TRANSACTIONS, 2020. MT-MK2019008.
[51] W. Chen, X. Ding, Y. Feng, X. Liu, K. Liu, Z. Lu, D. Li, Y. Li, C. Liu, X.-Q. Chen, Vacancy formation enthalpies of high-entropy FeCoCrNi alloy via first-principles calculations and possible implications to its superior radiation tolerance, J. Mater. Sci. Technol. 34 (2) (2018) 355–364.
[52] C. Li, J. Yin, K. Odbadrakh, B.C. Sales, S.J. Zinkle, G.M. Stocks, B.D. Wirth, First principle study of magnetism and vacancy energetics in a near equimolar NiFeMnCr high entropy alloy, J. Appl. Phys. 125 (15) (2019) 155103.
[53] M. Vilémová, K. Illková, Š. Csáki, F. Lukáč, H. Hadraba, J. Matějíček, Z. Chlup, J. Klečka, Thermal and oxidation behavior of CoCrFeMnNi alloy with and without yttrium oxide particle dispersion, J. Mater. Eng. Perform. 28 (9) (2019) 5850–5859.
[54] H. Ledbetter, Temperature behaviour of Young's moduli of forty engineering alloys, Cryogenics 22 (12) (1982) 653–656.
[55] M. Hayase, M. Shiga, Y. Nakamura, Spontaneous volume magnetostiction of Fe65 (Ni1− xMnx) 35 alloys, J. Phys. Soc. Jpn. 30 (3) (1971) 729–735.
[56] H. Zähres, M. Acet, W. Stam, E. Wassermann, Coexisting antiferromagnetism and ferromagnetism in Fe-Ni Invar, J. Magn. Magn Mater. 72 (1) (1988) 80–84.
[57] S. Kaya, Physics and Application of Invar-Honda Memorial Series on Materials Science No. 3, Maruzen, Tokyo, 1978, p. r4 [M].
[58] K. Sugita, N. Matsuoka, M. Mizuno, H. Araki, Vacancy formation enthalpy in CoCrFeMnNi high-entropy alloy, Scripta Mater. 176 (2020) 32–35.
[59] T. Holstein, H. Primakoff, Field dependence of the intrinsic domain magnetization of a ferromagnet, Phys. Rev. 58 (12) (1940) 1098.
[60] V. Shcherbakov, K. Fabian, N. Sycheva, S. McEnroe, Size and shape dependence of the magnetic ordering temperature in nanoscale magnetic particles, Geophys. J. Int. 191 (3) (2012) 954–964.
[61] M. Lucas, D. Belyea, C. Bauer, N. Bryant, E. Michel, Z. Turgut, S. Leontsev, J. Horwath, S. Semiatin, M. McHenry, Thermomagnetic analysis of FeCoCr x Ni alloys: magnetic entropy of high-entropy alloys, J. Appl. Phys. 113 (17) (2013) 17A923.